UXO Data Analysis

Final Report
SERDP Exploratory Development (SEED)
Project UXO-1216

Carl V. Nelson
Mary R. Keller
Dexter G. Smith

The Johns Hopkins University
Applied Physics Laboratory

March 29, 2002
STR-02-068

Report Documentation Page

Form Approved
OMB No. 0704-0188

1. REPORT DATE **29 MAR 2002**	2. REPORT TYPE	3. DATES COVERED **00-00-2002 to 00-00-2002**
4. TITLE AND SUBTITLE **UXO Data Analysis**		5a. CONTRACT NUMBER
		5b. GRANT NUMBER
		5c. PROGRAM ELEMENT NUMBER
6. AUTHOR(S)		5d. PROJECT NUMBER
		5e. TASK NUMBER
		5f. WORK UNIT NUMBER
7. PERFORMING ORGANIZATION NAME(S) AND ADDRESS(ES) **Johns Hopkins University,Applied Physics Laboratory,Johns Hopkins Road,Laurel,MD,20723-6099**		8. PERFORMING ORGANIZATION REPORT NUMBER
9. SPONSORING/MONITORING AGENCY NAME(S) AND ADDRESS(ES)		10. SPONSOR/MONITOR'S ACRONYM(S)
		11. SPONSOR/MONITOR'S REPORT NUMBER(S)
12. DISTRIBUTION/AVAILABILITY STATEMENT **Approved for public release; distribution unlimited**		
13. SUPPLEMENTARY NOTES		
14. ABSTRACT		
15. SUBJECT TERMS		

16. SECURITY CLASSIFICATION OF:			17. LIMITATION OF ABSTRACT	18. NUMBER OF PAGES	19a. NAME OF RESPONSIBLE PERSON
a. REPORT **unclassified**	b. ABSTRACT **unclassified**	c. THIS PAGE **unclassified**	**Same as Report (SAR)**	**17**	

1. Project Background

Currently, sensor systems exist that can detect and localize buried metal objects of a wide size and depth range. These sensors typically measure the active and/or passive magnetic properties of buried metal objects. In some cases, the sensor measures the dielectric contrast of the buried object (e.g., ground penetrating radar (GPR)). While current technology has shown the ability to detect these buried metal objects discriminating the UXO from metal objects that pose no risk, i.e. clutter, is still a major problem. These clutter objects represent a false alarm (FA) to the detection system. The time to remediate a site with a high clutter to UXO ratio is not cost effective. Discrimination of UXO from clutter, a reduction in the false alarm rate (FAR), would lower the site cleanup cost.

The report is divided into several sections. Section 2 describes the basic project objectives. Section 3 briefly describes the technical approach used in the UXO signature analysis and spatial signal processing. Section 4 summarizes the results of the project and Section 5 lists project recommendations. Section 6 summarizes some conclusions for the project while Section 7 makes recommendations for possible future work. The details of the project's efforts are documented in detail in the following Appendices:

- Appendix A: SPIE AeroSense 2002 Conference Paper
- Appendix B: Time Decay Analysis
- Appendix C: Holographic Imaging Analysis

2. Objective

The objective of the Johns Hopkins University Applied Physics Laboratory (JHU/APL) research was to investigate several different signal processing techniques to improve UXO discrimination capability. The signal and data processing techniques explored were:

- Time decay signature analysis using active electromagnetic induction (EMI) time-domain data.
- Spatial EMI data signal processing using a near-field holographic imaging technique.

A large amount of research has been done on target classification via time and frequency domain analysis with emphasis on simple target models[1]. Also, previous work used data from relatively low-bandwidth and low data resolution (number of data points per signature) time and frequency domain sensors. The present research effort examined target signature data from a relatively new high bandwidth, high data resolution time domain sensor [2,3]. In addition to the traditional signature analysis listed above, we looked at the data from the point of view of the sensor limitations and data characterization. The new sensor has the following characteristics:

- High bandwidth- ~ 100KHz
- Start time of decay signature after transmitter turn-off- ~ 25 µs
- Impulse response bandwidth of transmitter- ~ 1 MHz
- Data sample rate- 10 Msamples/s to 500 Ksamples/s
- Number of data points in signature record- 8,000

This research documents preliminary efforts to understand the new sensor as it applies to UXO signatures.

3. Technical Approach

3.1 Time Decay Signature Analysis

For a time-domain, eddy current response sensor system, a metal target can be modeled by defining a magnetic polarizability tensor that contains the target's primary magnetic decay response modes:

$$\overline{M} = \begin{pmatrix} M_x(t) & 0 & 0 \\ 0 & M_y(t) & 0 \\ 0 & 0 & M_z(t) \end{pmatrix} \tag{1}$$

where the diagonal components of the tensor are the time responses of the target to excitations in an orthogonal reference frame centered on the target. In an orthogonal XYZ coordinate system, $M_x(t)$ is the target's decay response to a magnetic field excitation in the X direction, $M_y(t)$ is the target's decay response to a magnetic field excitation in the Y direction, and $M_z(t)$ is the target's decay response to a magnetic field excitation in the Z direction. For an axially symmetric, or body of revolution (BOR), target, $M_x(t)$ and $M_y(t)$ are equal.

In the time-domain, one way to express the eddy current time decay response from metal target is to use:

$$V(t) = \delta(t) - \sum_i \left[A_i \exp\{-t/\tau_i\} \right] \tag{2}$$

where t is time, V(t) is the induced voltage in the receiver coil (proportional to M(t)) , $\delta(t)$ is the delta function, A_i are target amplitude response coefficients, and τ_i are the target's time constants. Thus, the sensor response to a metal target is a sum of exponentials with a series of characteristic amplitudes, A_i , and time constants, τ_i . These coefficients are a function of the metal target's physical, electrical and magnetic properties. Equations (1) and (2) form the theoretical basis of an EMI sensor's classification technique.

Equation (2) is one of several mathematical representations of a metal target's decay signature. When the target is a simple shape and non-ferrous, the decay signature can be represented as a single exponential to high accuracy. For complex metal targets and/or targets that have ferrous components, multiple exponential terms in equation (2) must be used to model the target signature. The complex nature of a target's signature is one reason we wish to explore methods for signature analysis that are relatively less complex to implement and understand physically.

3.2 Near-field Holography

In its simplest form, the near-field holographic technique is a combination of a straightforward EMI spatial measurement procedure and a unique treatment of the resulting

EM data. The area where the UXO is buried is illuminated with an active EM source located on or above the ground. The re- radiated EM fields from the target are measured at grid points in a horizontal plane at the surface of the ground in the vicinity of the buried target. The target response measured at the surface is first Fast Fourier transformed (FFT) into the frequency domain, so that the secondary magnetic fields re-radiated from the target are obtained as a function of frequency. (For sensors that are already in the frequency domain, this first step is not necessary.) The magnetic field, after being transformed into the frequency domain, is a complex function having both magnitude and phase. At a particular frequency, the magnetic fields at the individual grid points in the detection plane form a spatial distribution of the measured magnetic field in that plane. The spatial variation of the magnetic field depends on the characteristics of the buried target(s) and the distance from the target(s). This spatial distribution of the magnetic field at the detection plane is used to reconstruct the magnetic field distribution in the horizontal and vertical planes at various depths in the ground. By examining the reconstructed magnetic field distributions in the horizontal and vertical planes at various depths, the location of the target(s) in both the horizontal and the vertical dimensions can then be determined. The method is especially good at resolving multiple targets spaced close together.

4. Summary

Reference 4 and Appendix B describe in detail the EMI sensor and the data collection procedures. The field data analyzed in this report was collected at Blossom Point MD in September 2000. This section will summarize and discuss the projects results using this data and supplemental laboratory data.

4.1 Targets

To better appreciate the sometimes complex time decay signatures from the sensor, Figure 1 shows a picture of several typical UXO that were investigated in this project. The UXO are composed of both steel and aluminum components with complex shapes. We note that there is axial symmetry, but no vertical symmetry (top and bottom are different).

Figure 1: Typical UXO targets: 80 mm mortar, 60 mm mortar and 5 lb practice bomb

4.2 Understand the data and sensor

Figure 2 shows a summary of time decay signatures from several UXO targets plotted on a log-log graph. This figure illustrates a number of data and sensor issues. Aside from the clear differences in signature with respect to target type and orientation (which hopefully allows us to classify the target), several items to note in the Figure are:

- Time ranges- Data start time is about 20 μs to greater than 10 ms. This figure illustrates that wide time range of signatures. There is structure in the decay signature throughout the 4 orders of magnitude in time.
- Signal amplitudes- The voltage from the sensor spans about 4 orders of magnitude.
- Gain and saturation issues- Most EMI sensors operate at their maximum gain. A large target buried at a shallow depth will tend to saturate such a sensor. A properly designed sensor will adjust its gain to not saturate its amplifiers when a large target is encountered.
- Multiple time windows- Small targets typically decay more rapidly than large targets. Therefore, a properly designed sensor should be capable of operating with different sample rates over different time windows. For example, in Figure 2, the “golf-ball bomblet” decays to the sensor noise floor at about 300 μs. To optimize data collection the sensor would collect data over this time window. For the case of the vertical 80 mm mortar shell, the 16 ms time window was not wide enough to collect the entire decay signature before the sensor noise floor was reached. There is still signature information after 16 ms that is lost by the non-optimized measurement.

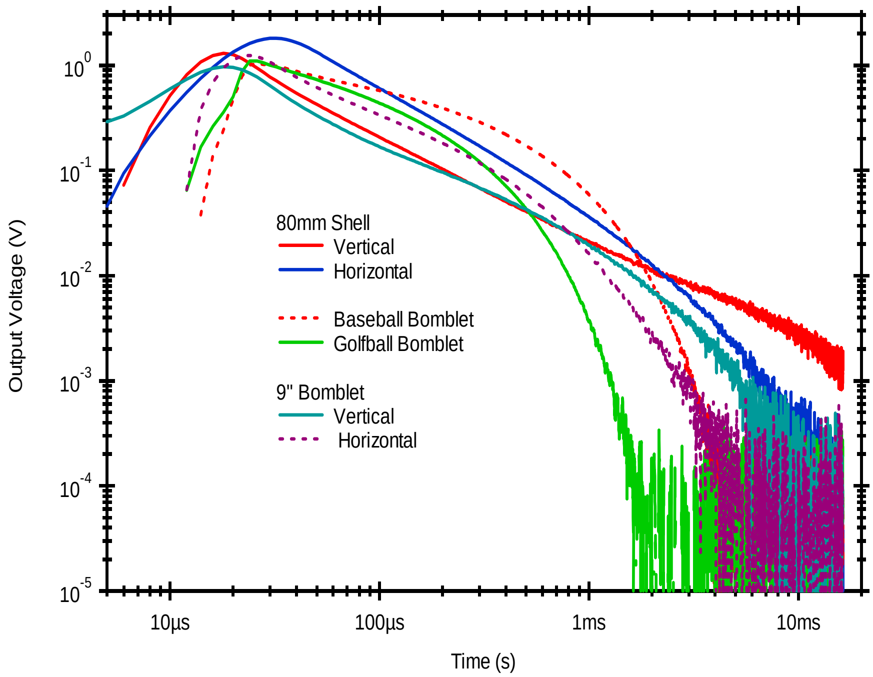

Figure 2: Sample UXO time decay signature data.

4.3 Spatial Time Decay Signature Data

Figure 3 illustrates typical spatial decay target signature data that was analyzed by the project from a horizontally oriented 81 mm mortar. The direction and magnitude of the excitation magnetic field spatially varies as the mortar moves from the center of the antenna as shown in the Figure. Figure 4 shows data from Figure 3 normalized to 1 at 10 µs. This normalization approach shows the relative time decay character of a signature without the need of parameterization. The concept of data normalization and using the normalized signatures as templates will be discussed below. The amplitude of the time decay signatures changes, however, since the mortar's orientation is symmetric with respect to the field changes, as expected, the normalized time decay does not change. Note that the target decay signatures for the center positions span approximately 3 decades in amplitude and 2 decades in time.

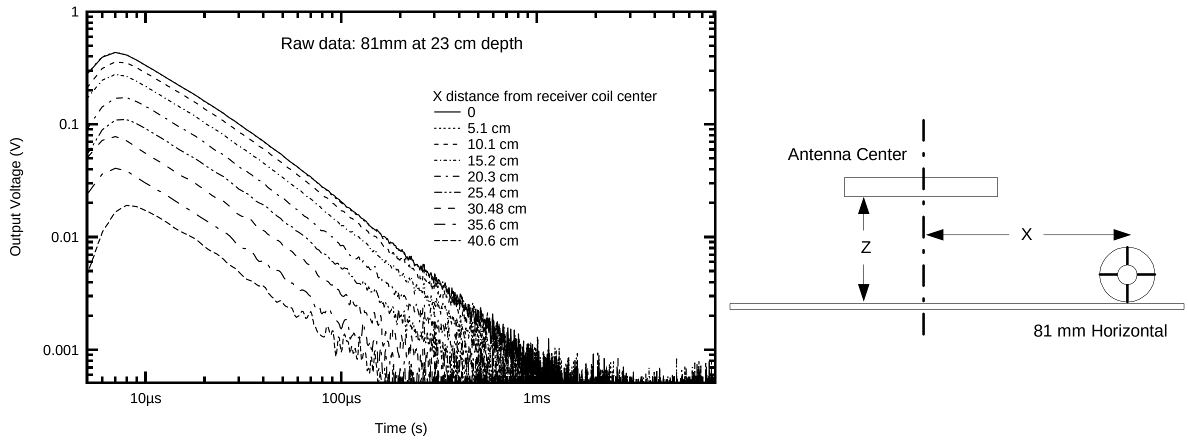

Figure 3: Spatial time decay signatures from a 81 mm mortar

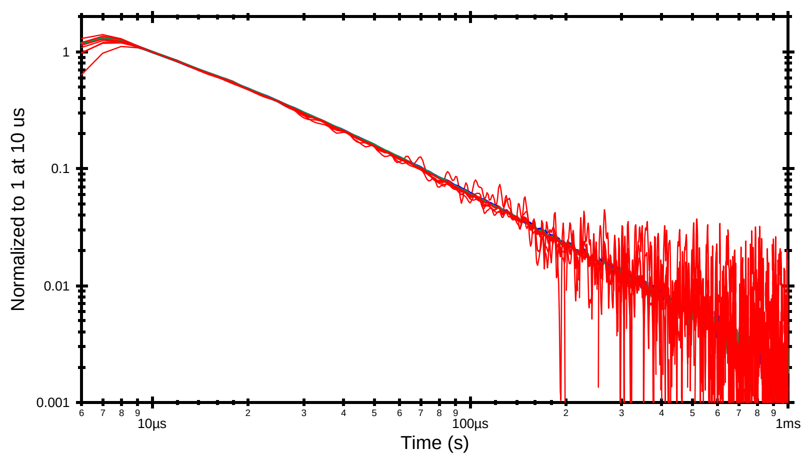

Figure 4. Overlay of 8 spatial 81 mm mortar (horizontal orientation) time decay signatures normalized to 1 at 10 µs.

Example normalized time decay target signatures for an 61 mm mortar in different offset positions relative to the center of the sensor's antenna are shown in Figure 5. The target and sensor antenna depth separation was about 16 cm. To show the relative time decay, the data were normalized to 1 at 30 µs. The plots show fairly substantial differences in the decay signature when the vertically mounted mortar is moved from directly under the antenna (X = 0 cm) to an offset distance of 30.5 cm. It is interesting to note that the X = 30.5 cm time decay signature is almost identical to the time decay signature of a horizontally oriented shell.

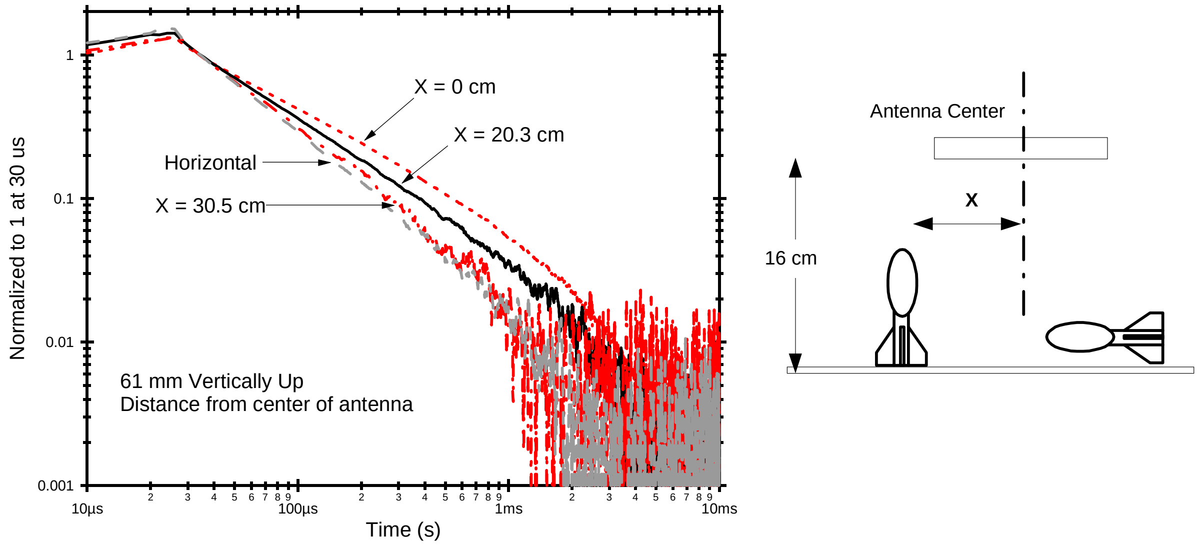

Figure 5: Normalized time decay signatures for 61 mm mortar in different orientations.

Figure 6 shows normalized time decay signatures from an 61 mm mortar along the centerline of the antenna in two orientations; vertical up and vertical down. Figure 6 shows an interesting feature: there is relatively little difference in the time decay signature when the mortar is pointing up or down. The feature is interesting because one would expect the time decay signatures to be different since the head of the mortar is mainly composed of steel and the tail is mainly composed of aluminum (tail fin). When the steel head is close to the antenna, we would expect its decay signature would dominate. When the aluminum tail fin is close to the antenna, we would expect its decay signature would manifest itself more dramatically. There is a small apparent difference in the time decay signature between 500 μs and 2 ms, but we cannot rule out statistical variation in the signal due to sensor and target misalignment. On the one hand this result is encouraging because it means that the vertical polarization tensor is symmetric between up and down orientation of the target: Target classification will be somewhat easier. But, on the other hand, it goes against ones intuition. One must all note, that the relative EMI response from steel is much larger than the EMI response from aluminum. This may account for the apparent signal properties.

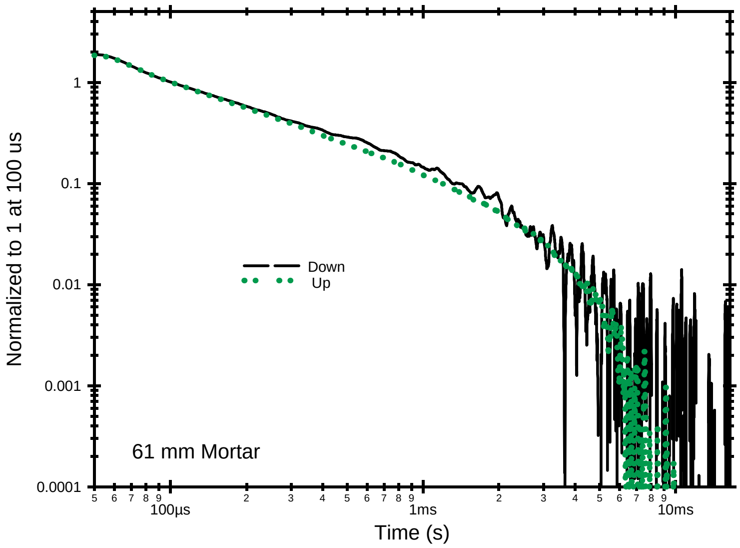

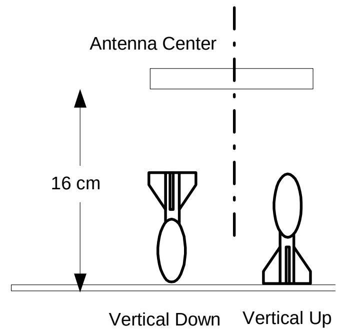

Figure 6: Normalized time decay signatures for 61 mm mortar in up and down orientations along antenna centerline.

4.4 Time Decay Parameterization

Among the many analysis approaches for target classification[5], a compact representation of the data has the attractive feature of a minimum number of target classification parameters. The high signal to noise ratio (SNR) of the UXO data collected in these experiments permitted the use of a straightforward nonlinear Levenberg-Marquardt[6] least-squares fitting of multiple exponentials over discrete regions of the target time decay. Representing the data as a sum of exponentials (as illustrated in equation (2)) allows one to possibly characterize a target with as few as one parameter per target axis, i.e., the decay time constant for that axis.

Figure 7 shows an initial attempt to fit a single exponential to the time decay signature of a horizontal 81 mm mortar at a depth of 9 cm. The time decay signature covers approximately three orders of magnitude in amplitude and one and a half decades in time. The dashed over-plotted line is the best-fit to the single exponential. Even though the fit has a χ^2 of 8.3e-6, it is clearly inadequate to describe the properties of the time decay. To improve the fit, we took the same raw data and fitted it with a three- exponential curve fit equation. An over-plot similar to Figure 7 would show nothing but the raw data, since the new fit curve matches the raw data very well. Instead, Figure 8 shows the residual differences between the fitted and raw data. The small magnitudes of the residuals indicate that the fits are nearly indistinguishable from the original data.

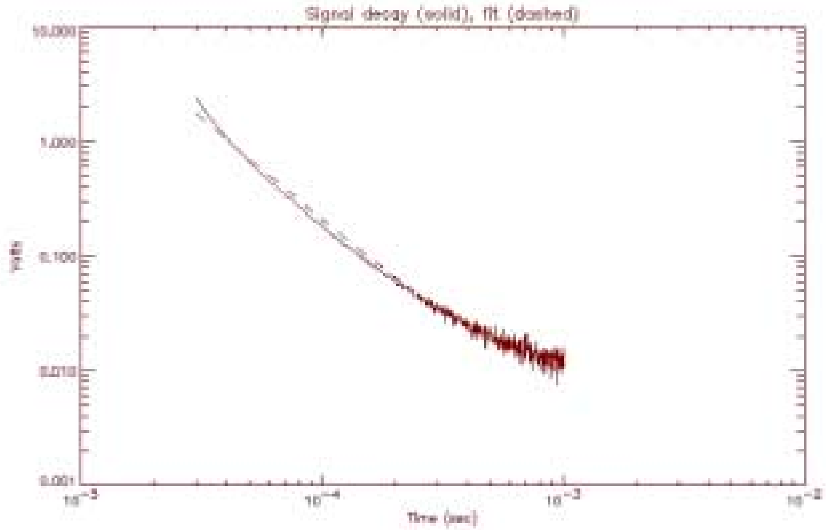

Figure 7: Single exponential fit to time decay of an 81 mm mortar shell at a depth of 9 cm.

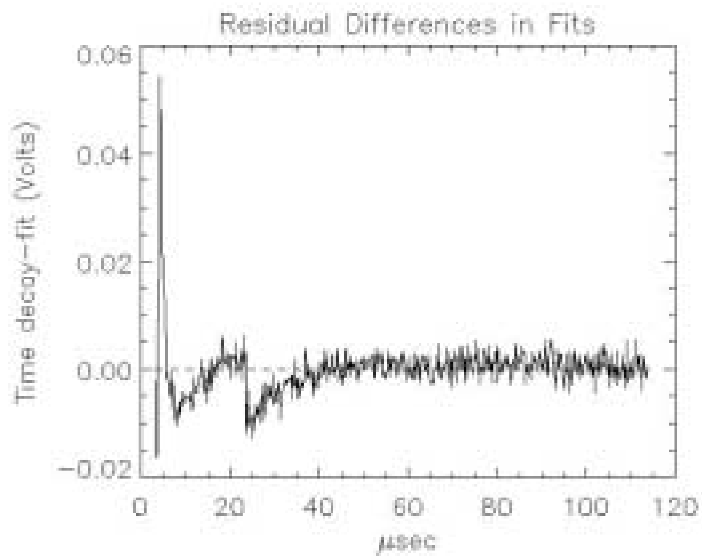

Figure 8: Residual differences for multiple exponential fits to the same time decay as in Figure 7. Note that the three exponential fits, outside of initial transients, are virtually indistinguishable from the data being fitted.

Figure 9 shows a plot of the first versus the second exponential for three targets, two mortar shells and an ellipsoidal egg. The sensor-to-target depths were: 81mm mortar shell, 9 cm; 60mm mortar shell, 10 cm; and, ellipsoidal egg, 8 cm. These target data are were chosen because we had multiple time decays under identical conditions, and this allowed the development of ensemble statistics for the targets. The bars on the points represent the standard deviation in the exponential fits, all of which have χ^2 of less than $5x10^{-9}$. The plot shows that with sufficiently high signal-to-noise and careful attention to the fitting of the data, target parameterization can proceed using straightforward techniques. Additional information is available in the fitting process, namely the amplitudes of the exponential terms. For simplicity of presentation, we have chosen not to present this additional information in a multi-dimensional graph. The two exponential terms, for these target types, appear to have

sufficient separation in this parameter space for some target discrimination. One would naturally use every bit of signature characterization information in a target parameterization or classification scheme.

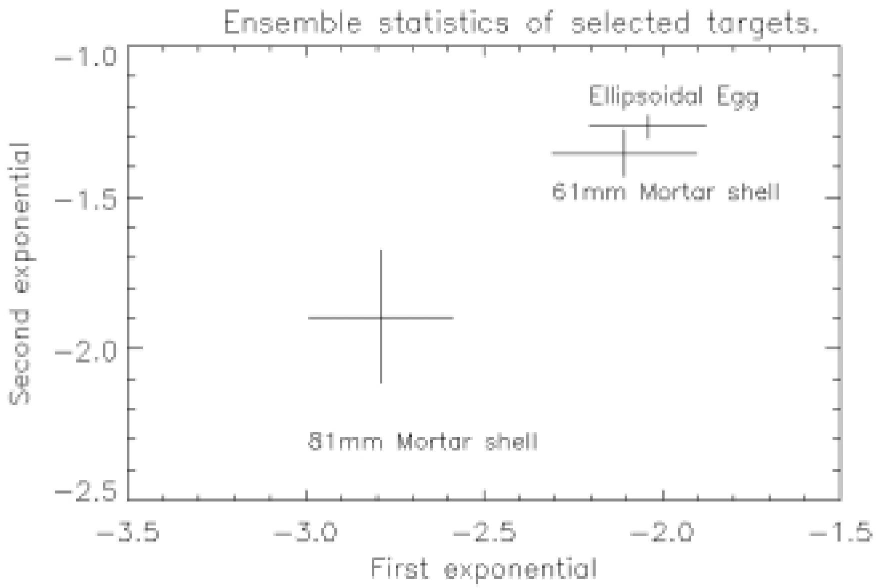

Figure 9: Comparison of ensemble-averaged first and second exponentials for different types of UXO and clutter. The length of the lines represents the standard deviation of each ensemble average.

In addition to the exponential curve-fitting algorithms, we also analyzed the time decay data with a T^{-N} curve fitting routine. Data are presented in the Appendix.

The usefulness of time decay signature parameterization can be summarized:

- Compact representation of data- library of target signature estimates
- Assist in classifier algorithm development- easy to use in theoretical development
- Assist in sensor development- easy first-order modeling
- Assist in modeling and simulation development- easy first-order modeling
- Multiple Window Analysis- quick and easy way to calculate window values

4.5 Normalized decay signatures for classifier templates

Many of the targets illustrated above show complex time decay signatures that are not easily parameterized or put into a convenient signal processing form. One way that simplifies the parameterization process is to just use the target's own signature as the signal processing template. The time decay signature of a target is an inherent property of the target (orientation issue resolved by equation (1)); once excited by the magnetic impulse from the sensor's transmitter coil, the target's magnetic field decays uniformly in space. The absolute amplitude of the time decay response does not govern the target characterization process. The relative time decay signature is the important feature we wish to extract. To do so, we

normalized to 1 at some convenient time the decay signature. For the cases of small metal target, the amplitude is normalized at an early time after transmitter turn-off. For large targets, with long decay times, we can select one or more normalization times, for target characterization over many orders of magnitude of time.

4.6 Holographic Imaging

Conventional holography relies on illumination of targets that are large relative to the wavelength of the imaging radiation. In the case of the ETD system, not only are the sensor wavelengths much larger than the targets being detected, the UXO is located in the near-field of the sensor. For such situations, near-field imaging, making use of evanescent wave properties, can provide depth and position localization for a target. Back-propagation techniques for evanescent waves have been developed for many applications[7,8] and will not be discussed in depth for this paper. It is sufficient to note that with the back-propagation technique, energy will go to zero, or minimize, at the depth of the source of the evanescent waves. It should be possible, then, to take time-decay data from the ETD sensor, extract values at specific time decays collected over an X-Y spatial grid, and predict target depths using evanescent wave back-propagation analyses. Figure 10 shows the depth slices in 0.5 cm increments. Figure 11 shows evanescent wave energy, integrated over the space of the x-y grid of data, as a function of depth, as calculated from the back-propagation algorithm. At the measured depth (8 cm) of the target, an ellipsoidal egg, the energy minimizes, just as theory predicts it should. More detailed results of the holographic analysis is described in Appendix D.

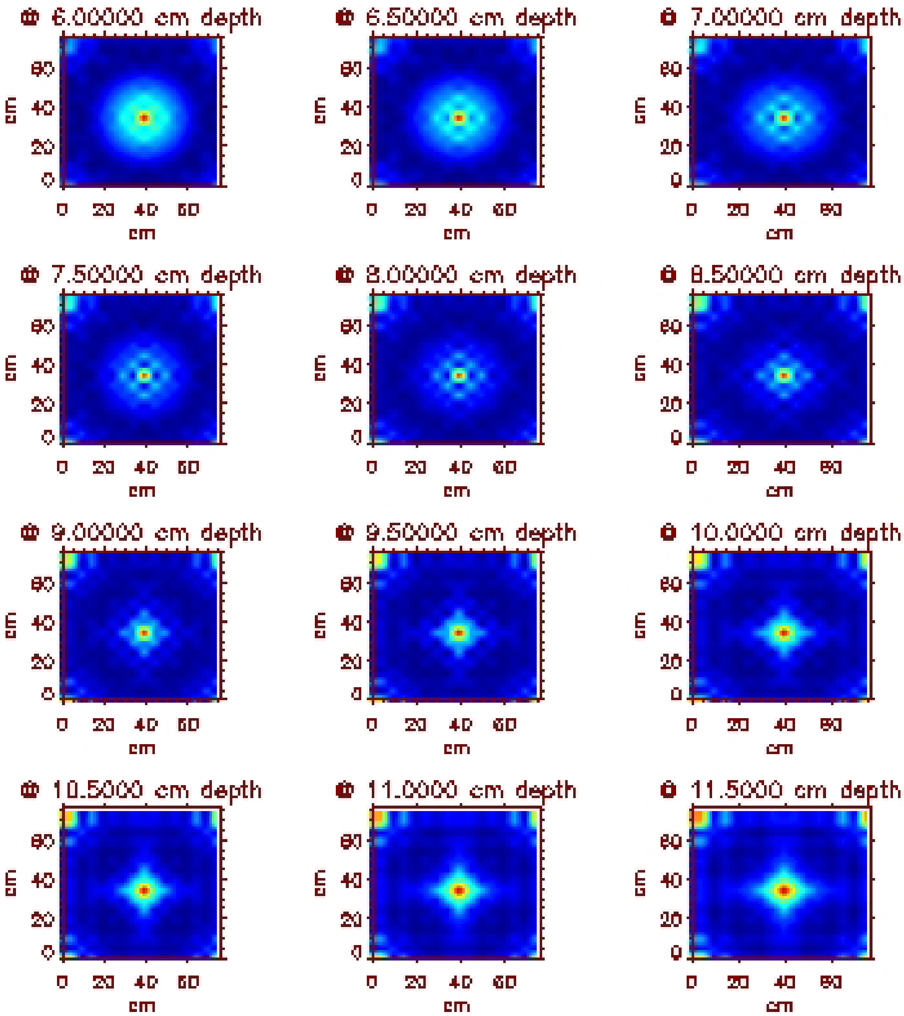

Figure 10. Depth reconstruction over a steel egg with a sensor to target distance of 8 cm. Depth slices 6 to 11.5 cm.

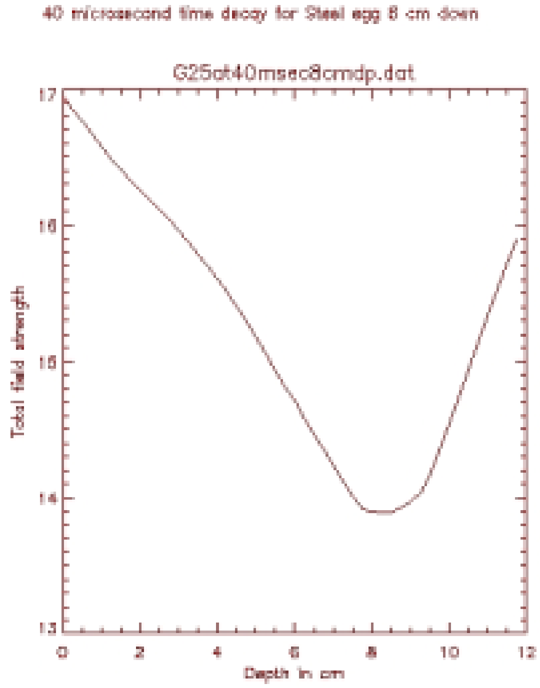

Figure 11: Total integrated energy as a function of depth from an ellipsoidal egg 8 cm below the ETD antenna. Evanescent wave back-propagation theory predicts the energy should minimize at the depth of the target.

5. Project Accomplishments

- Conference/Symposium Proceedings Papers: **Wide Bandwidth, Time Decay Signatures from UXO Targets,** by C. V. Nelson and M. R. Keller, presented at the SPIE AeroSense 2002 Conference, April 4, 2002, Orlando, Florida. The proceedings paper is 4742-87, and will be available in printed form when the proceedings are published in September 2002
- A complete description of the Levenberg-Marquardt non-linear analysis and the near-field holographic imaging analysis are given in Appendix B.
- Time decay signature analysis and parameterization library for a large number of UXO targets
- Holographic processing of UXO targets signatures

6. Conclusions

Time Decay Analysis: The Levenberg-Marquardt non-linear analysis, when applied using the algorithms developed to define the time decay and the number of poles necessary to describe that time decay, permits discrimination between UXO's and clutter, and different types of UXO's.

Near-Field Holography: Initial work with simulated targets has illustrated potential difficulties with near-field holographic imaging techniques (see Appendix D). The surface

field needs to be sampled carefully, based on the characteristics of the target beneath, for optimum depth retrieval. Even with the best sampling intervals selected, the holo-graphic code (holocode) predicted a depth that was usually slightly less than the true depth of the target. Guo [7] found similar under-predictions in their initial work with the holocodes. These conclusions hold whether the simulated target was a single dipole at depth, or multiple dipoles in complex configurations. When the dipoles were placed at different depths, the holocode could only retrieve the depth of the top dipole, but not any further information about the target itself.

Test data were acquired with two different experimental systems. These also reveal potential difficulties with straightforward near-field holographic imaging techniques. A frequency-integrating system, although portable in design, and with an antenna useful in restricted locations, could not discriminate between spurious signals and targets. Further, it was sensitive to electrical sources at a distance from the sensor itself (light fixtures several meters away from the antenna), and, with the transmit and receive antenna co-located, suffered from the generation of a non-uniform transmitter field over steel targets. A EMI system assembled for laboratory work, while yielding better results with a large fixed transmitter antenna and a mobile receiver antenna, still suffered from too small a uniform transmitted field to achieve the best results over a wide variety of targets.

Field data acquired at Blossom Point show the same deficiencies as were predicted by the target simulations and illuminated by the test data. When the target was of a uniform composition and of simple structure, straightforward application of the holocodes yielded high-quality results. Over targets of complex shapes, not even TEMID time decay information selected on the basis of the knowledge of the composition of the target was sufficient to permit retrieval of the target depth or orientation.

7. Recommendations

7.1 Time Decay Analysis

SERDP has approved a follow-on project in the 3-D steerable antenna (Proposal UX3-077P). The analysis techniques and sensor parameter understanding developed in the project has helped JHU/APL to develop this 3-D antenna proposal. The information on the poles of UXO's and clutter acquired in this study will provide a first cut for target identification of unknown targets and has assisted in modeling efforts. Continued work and support in this area is recommended to further the development and understanding of UXO signatures and their relationship with the sensors that are developed to measure their properties.

7.2 Near-Field Holography

The Near-field holographic technique shows promise for better defining the depth of a target. The technique has also shown the potential to resolve multiple, closely spaced metal targets. If measurements like these are to be repeated in the future, it would be advantageous to build a transmitting antenna with spatial dimensions at least three times the size of the largest possible target. This decreases the portability of the detection system, but would eliminate

problems with the field changing over the edge of the target. In short, the optimum configuration of transmitter and receiver antennas for all possible targets remains to be determined. Continued work and support in this area is recommended to further the development technique for UXO classification.

One of the more ambitious objectives of the project was to take the holographic imaging software and merge it with the time decay information available from the EMI sensor system. When the target was a simple shape and of uniform composition, the EMI sensor system performed reasonably well, given the straightforwardness of the holocode software, in retrieving depth information about rebar and UXO-like targets. However, once the targets had complex shapes or were composites of different materials, even the best combination of time decay information was insufficient to yield an accurate estimate of the target depth. Further work along these lines was not pursued as a part of this study, which sought to apply relatively straightforward techniques for target determination and depth retrieval. In future work, it would be advantageous to examine integrated time decay information based on possible compositions of the materials of the target to improve depth retrievals. Further, a more robust holographic imaging algorithm that does not depend on modeling targets as dipole combinations remains to be developed to retrieve further information about targets at depth.

References

1. I. J. Won, Dean A. Keiswetter, and Thomas H. Bell, “Electromagnetic Induction Spectroscopy for Clearing Landmines,” IEEE Trans. Geoscience and Remote Sensing, **Vol. 39**, No. 4, pp 703-709, April 2001

2. Carl V. Nelson, Charles B. Cooperman, Wolfger Schneider, Douglas S. Wenstrand, and Dexter G. Smith, “Wide Bandwidth Time-domain Electromagnetic Sensor for Metal Target Classification,” IEEE. Trans. Geoscience and Remote Sensing, **Vol. 39**, No. 6, pp 1129-1138, June 2001.

3. Carl V. Nelson and Toan B. Huynh, “Wide Bandwidth, Time Decay Responses from Low-metal Mines and Ground Voids,” SPIE, FL, 2001. Proceeding of SPIE, Detection and Remediation Technologies for Mines and Minelike Targets, Orlando, FL, 16-20 April 2001.

4. C. V. Nelson, M. A. Sandler, T. B. Huynh, S. A. Ross and T. M. Higgins, “Blossom Point UXO Field Test Results.” 20 October 2000 STX-00-062, Final Report to SERDP.

5. Tatum, S.L., and L.M. Collins, “A Comparison of Algorithms for Subsurface Target Detection and Identification Using Time-domain electromagnetic Induction Data,” IEEE Transactions on Geoscience and Remote Sensing, **Vol. 39**, no. 6, pp. 1299-1306, 2001.

6. More, J.J., "The Levenberg-Marquardt Algorithm: Implementation and Theory", in *Numerical Analysis,* ed. Watson, G. A., *Lecture Notes in Mathematics 630*, Springer-Verlag, 1977.

7. Guo, Y., H. W. Ko, and D. M. White, "3-D localization of buried objects by near-field electromagnetic holography", Geophysics, **vol. 63**, no. 3, pp. 880-889, 1998.

8. Guo Y., C. V. Nelson and D. M. White, " 3-D Localization Using Time-domain Electromagnetic System," *UXO Forum 1996*, pp. 325-331, March 26-28, 1996, Williamsburg, VA..

Appendices

- Appendix A: SPIE AeroSense 2002 Conference Paper
- Appendix B: Time Decay Analysis
- Appendix C: Holographic Imaging Analysis